Heterovalent and A-atom effects in $A(B'B'')O_3$ perovskite alloys

L. Bellaiche, J. Padilla and David Vanderbilt
Department of Physics and Astronomy,
Rutgers University, Piscataway, New Jersey 08855-0849, USA
(August 24, 1998)

Using first-principles supercell calculations, we have investigated energetic, structural and dielectric properties of three different $A(B'B'')O_3$ perovskite alloys: $Ba(Zn_{1/3}Nb_{2/3})O_3$ (BZN), $Pb(Zn_{1/3}Nb_{2/3})O_3$ (PZN), and $Pb(Zr_{1/3}Ti_{2/3})O_3$ (PZT). In the homovalent alloy PZT, the energetics are found to be mainly driven by atomic relaxations. In the heterovalent alloys BZN and PZN, however, electrostatic interactions among B' and B'' atoms are found to be very important. These electrostatic interactions are responsible for the stabilization of the observed compositional long-range order in BZN. On the other hand, cell relaxations and the formation of short Pb–O bonds could lead to a destabilization of the same ordered structure in PZN. Finally, comparing the dielectric properties of homovalent and heterovalent alloys, the most dramatic difference arises in connection with the effective charges of the B' atom. We find that the effective charge of Zr in PZT is anomalous, while in BZN and PZN the effective charge of Zn is close to its nominal ionic value.

PACS numbers: 77.84.Dy, 71.15.Mb, 71.20.Be, 71.23.-k

I. INTRODUCTION

Simple perovskite compounds have the chemical formula ABO_3. In the cubic phase, the oxygen atoms form a cubic lattice of corner-sharing octahedra with the B cations at their centers, while the A cations form a second interpenetrating cubic sublattice located at the 12-fold coordinated sites between octahedra. Interestingly, most of the perovskite compounds that are of greatest technological interests are not simple systems, but rather $A(B'B'')O_3$ alloys with two different kinds of B atoms. Examples include the $Pb(ZrTi)O_3$ alloys that are currently used in piezoelectric transducers and actuators[1–3]. Other examples include $Ba(MgNb)O_3$ for high-frequency applications[4], and $Pb(MgNb)O_3$ and $Pb(ZnNb)O_3$ which exhibit extraordinarily high values of the piezoelectric constants when alloyed with $PbTiO_3$[5].

From a chemical point of view, two classes of $A(B'B'')O_3$ compounds can be distinguished: homovalent *vs.* heterovalent alloys. In homovalent alloys, the two B atoms belong to the same column of the periodic table. The $A(B'_xB''_{1-x})O_3$ alloys can thus have a composition x continuously ranging from 0 to 1. A typical example of such a homovalent alloy is $Pb(Zr_xTi_{1-x})O_3$. On the other hand, there is a unique stoichiometry in heterovalent alloys, since the two B atoms do not belong to the same column of the periodic table. Typical examples of heterovalent alloys are $Pb(Zn_{1/3}Nb_{2/3})O_3$, $Ba(Zn_{1/3}Nb_{2/3})O_3$, $Pb(Mg_{1/3}Nb_{2/3})O_3$, $Ba(Mg_{1/3}Nb_{2/3})O_3$, and $Pb(Sc_{1/2}Ta_{1/2})O_3$.

While many first-principles calculations have been performed to understand and predict properties of simple ABO_3 perovskite systems (see Ref.[6–8] and references therein), only a few studies have investigated alloy properties via accurate *ab-initio* techniques. For example, ferroelectric effects in PZT have been studied[9], and energetics of long-range order structures of homovalent or heterovalent alloys have been investigated[10–13]. These recent studies provide a useful understanding of the microscopic behavior of perovskite alloys, but they do not give a simple picture of the consequences of heterovalency on the energetics and properties of the alloys. For example, one may wish to compare the driving mechanisms responsible for the energetics of homovalent and heterovalent alloys. It is also unclear how the chemical difference between homovalent and heterovalent alloys affects interatomic distances and dielectric properties.

Another aspect that is poorly understood is the effect of the A-atom identity on properties of heterovalent alloys. For example, many Ba-compounds including $Ba(Mg_{1/3}Nb_{2/3})O_3$ (BMN)[4], $Ba(Zn_{1/3}Nb_{2/3})O_3$ (BZN)[14], $Ba(Zn_{1/3}Ta_{2/3})O_3$ (BZT)[15,16], $Ba(Mg_{1/3}Ta_{2/3})O_3$ (BMT)[17], $Ba(Sr_{1/3}Ta_{2/3})O_3$ (BST)[17] and $Ba(Ni_{1/3}Nb_{2/3})O_3$ (BNN)[18], adopt a structure with long-range compositional order in which one plane of B' atoms alternates with two planes of B'' atoms along the [111] direction. We shall refer to this as the $1{:}2_{[111]}$ structure. On the other hand, weak X-ray reflections have been detected in various Pb-compounds, such as $Pb(Mg_{1/3}Nb_{2/3})O_3$ (PMN)[19–21] and $Pb(Mg_{1/3}Ta_{2/3})O_3$ (PMT)[22], that are indicative of a rocksalt-like 1:1 ordering of B'-rich and B''-rich sites on the B sublattice. We will refer to this as the $1{:}1_{[111]}$ structure, since it can be regarded as consisting of a simple alternation of planes of B'-rich and B''-rich sites along [111]. The nature and strength of the atomic ordering have been shown to be crucial for the properties of this class of alloys.

Understanding heterovalent and A-atom effects can also be very useful for building an accurate effective Hamiltonian that can extend the reach of first-principles calculations by retaining only the physically relevant degrees of freedom[11]. Effective Hamiltonian approaches have been developed in the past for simple perovskite systems. When constructed from first-principles calculations, they have proven to be very successful both for reproducing phases transition sequences[23–25], and for studying ferroelectric domain walls[26] as well as finite-temperature dielectric and electromechanical properties[27–29]. An effective Hamiltonian for a perovskite alloy should include both compositional and structural degrees of freedom. A good starting point for treating the former may be the simple model of Ref.[30]. By focusing on electrostatic effects, this model successfully reproduces the compositional long-range order observed in a large class of complex heterovalent perovskite alloys. However, in order to augment this model with a description of structural relaxations, we are motivated to understand the role of such relaxations in the energetics and the dielectric properties of these materials.

In the present study, we investigate both heterovalent and A-atom effects in an important class of perovskite alloys using first-principles techniques applied to ordered supercells. To study heterovalent effects, we compare the computed properties of $Pb(B'B'')O_3$ alloys for the cases of homovalent vs. heterovalent B-site substitution. With regard to A-atom effects, we are mainly interested in the differences between Pb compounds and other divalent-A compounds. While we find that the energetics of homovalent alloys are mainly driven by atomic relaxations, we confirm that the electrostatic interactions are extremely important to understand the energetic and other properties of heterovalent alloys. For example, electrostatic interactions are mainly responsible for the long-range order seen in heterovalent Ba-compounds. In addition, we find that the formation of short Pb–O bonds in heterovalent $Pb(B'B'')O_3$ alloys could help in destabilizing the structure suggested by electrostatic considerations alone. Finally, the present study also emphasizes that the dielectric properties of homovalent and heterovalent alloys can differ considerably. For example, the effective charge of the B′ atom is found to be anomalous in homovalent alloys, while it is close to its nominal value in heterovalent alloys.

Specifically, we have chosen three compounds for study. These are the homovalent $Pb(Zr_xTi_{1-x})O_3$ (PZT) system and the heterovalent $Pb(Zn_{1/3}Nb_{2/3})O_3$ (PZN) and $Ba(Zn_{1/3}Nb_{2/3})O_3$ (BZN) systems. To facilitate direct comparison between the homovalent and heterovalent alloys, we choose the same composition $x = 1/3$ for PZT as for PZN and BZN. Note that in all three alloys the larger B atom (Zn or Zr) is the minority species, while the smaller one (Nb or Ti) is the majority.

All the supercells studied in the present article retain inversion symmetry, thus preventing the occurrence of ferroelectricity and piezoelectricity. While the Pb compounds PZN and PZT do exhibit ferroelectricity at low temperature, many interesting features (such as short Pb–O bonds[31]) appear in the paraelectric phase of these compounds. Moreover, the atomic ordering on the B sublattice, which is a focus of the present work, is determined at growth temperatures well above the ferroelectric-to-paraelectric transition temperature. For the purpose of understanding the intrinsic differences between homovalent and heterovalent alloys, and between heterovalent alloys with two different A atoms, we thus decided not to relax the inversion-symmetry constraint.

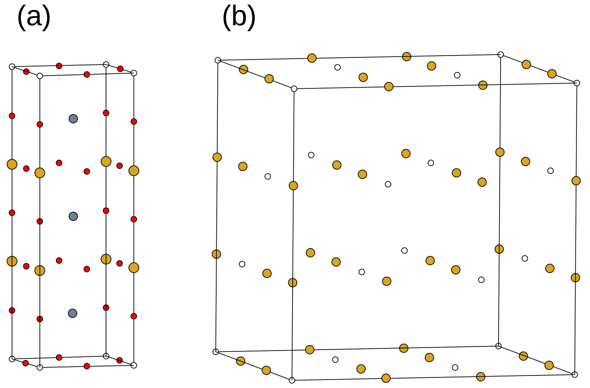

FIG. 1. (a) The $1{:}2_{[001]}$ $A_3(B'B''_2)O_9$ supercell. The succession of planes from bottom to top (i.e., progressing along [001]) is (B′,O), (Pb,O), (B″,O), (Pb,O), (B″,O), (Pb,O)... (b) B-site atomic ordering in the $1{:}2_{[111]}$ structure, illustrated within a large box aligned with the cartesian axes. The succession of planes progressing along the [111] direction is (B′), (Pb,O), (B″), (Pb,O), (B″), (Pb,O)...; only B′ and B″ atoms (small open and large filled circles respectively) are shown here.

II. METHODS

We limit ourselves to the two ordered superlattice structures shown in Fig. 1. These 15-atoms supercells consist of one B′ plane alternating with two B″ planes along either the [001] direction (Fig. 1a) or the [111] direction (Fig. 1b). The structure shown in Fig. 1a will be denoted as $1{:}2_{[001]}$. As previously indicated, $1{:}2_{[111]}$ denotes the structure shown in Fig. 1b. The lattice vectors of the $1{:}2_{[001]}$ structure are $\mathbf{a}_{[001]} = a_0[1,0,0]$, $\mathbf{b}_{[001]} = a_0[0,1,0]$, and $\mathbf{c}_{[001]} = \xi a_0[0,0,3]$, where a_0 is the lattice parameter and ξ is the ordered-related axial ratio. The ideal $1{:}2_{[001]}$ structure exhibits the tetragonal 4/mmm point group. On the other hand, the point group of the ideal $1{:}2_{[111]}$ structure is $\bar{3}$m, and its lattice vectors are $\mathbf{a}_{[111]} = a_0[1,0,-1]$, $\mathbf{b}_{[111]} = a_0[-1,1,0]$, and $\mathbf{c}_{[111]} = \xi a_0[1,1,1]$, where a_0 is the lattice parameter and ξ is the ordered-related axial ratio. We will retain the ideal group symmetry in both structures. The two B″ atoms are then equivalent by symmetry in both structures. Of the three A atoms in the cell, the two A atoms located between a B′ and a B″ plane are equivalent to each other and are free to move along the compositional

([001] or [111]) direction. These atoms will be denoted A_1 below. The third A atom, which we denote A_2, lies on the mirror plane between the two B'' planes and is forced by symmetry to remain undisplaced.

We perform local-density approximation (LDA) calculations on the above supercells using the Vanderbilt ultrasoft-pseudopotential scheme[32]. As detailed in Ref.[33], a conjugate-gradient technique is used to minimize the Kohn-Sham energy functional. The ultrasoft-pseudopotential approach has two major advantages. First, it allows for the generation of exceptionally transferable pseudopotentials because of its use of multiple reference energies during the construction procedure. Second, a modest plane-wave cutoff can be used, thus also allowing us to include the semicore shells in the valence for all the metals considered. Technically, we chose the plane-wave cutoff to be 25 Ry, which leads to converged results of physical properties of interest[33] using roughly 2,700 plane waves per 15-atom supercell. The Pb $5d$, Pb $6s$, Pb $6p$, Zr $4s$, Zr $4p$, Zr $4d$, Zr $5s$, Ti $3s$, Ti $3p$, Ti $3d$, Ti $4s$, Zn $3d$, Zn $4s$, Nb $4s$, Nb $4p$, Nb $4d$, Nb $5s$, O $2s$ and O $2p$ electrons are treated as valence electrons in the present study. Consequently, our calculations include 122, 134 and 132 electrons per cell in BZN, PZN and PZT, respectively. We use the Ceperley-Alder exchange and correlation[34] as parameterized by Perdew and Zunger[35]. A (6,6,2) Monkhorst-Pack mesh[36] was used for the $1{:}2_{[001]}$ structure, corresponding to six k-points in the irreducible wedge of the Brillouin zone, and providing a desirable exact mapping onto the (6,6,6) mesh of the primitive 5-atom simple perovskite cell[33]. A (3,3,3) Monkhorst-Pack mesh[36] was used for the $1{:}2_{[111]}$ structure, corresponding to 10 k-points in the irreducible zone of the $1{:}2_{[111]}$ structure. We checked that this mesh leads to converged results by noticing that the total energy of PZT $1{:}2_{[111]}$ structure computed with the (4,4,3) and the (3,3,3) meshes differed by less than 0.002 eV.

The lattice parameter a_0, the "ordered-related" axial ratio ξ, and those atomic displacements consistent with the symmetries of the ideal structures were fully optimized by minimizing the total energy and the Hellmann-Feynman forces, the latter being smaller than 0.04 eV/Å at convergence.

The dynamical effective charge of an atom was determined by calculating the difference in polarization between the ground state structure and a structure in which the given atom was displaced slightly along the compositional direction, the first-order variation of the polarization with atomic displacement being the dynamical effective charge Z^*. We follow the procedure introduced in Ref.[37] which consists in directly calculating the spontaneous polarization as a Berry phase of the Bloch states. Technically, we use roughly 2,000 Bloch states to assure a good convergence of the effective charges.

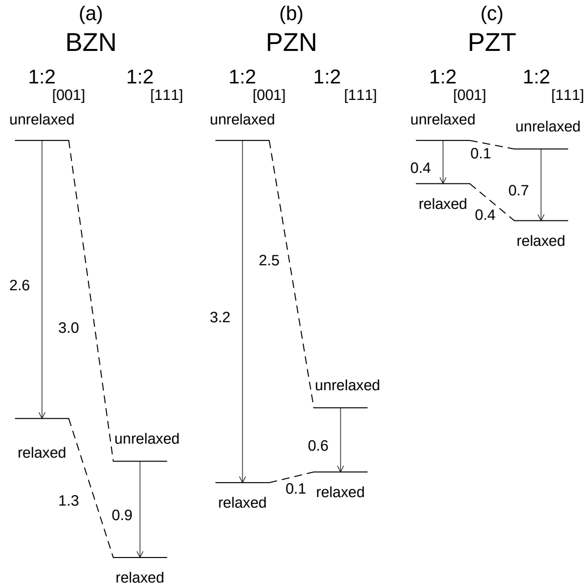

FIG. 2. Illustration of total-energy differences for (a) BZN, (b) PZN, and (c) PZT. The zero of total energy is arbitrarily chosen to be that of the unrelaxed $1{:}2_{[001]}$ structure.

III. RESULTS:

A. Energetics

Figure 2 illustrates the computed energetics for the BZN, PZN, and PZT cases, showing the energy differences with and without relaxations, and for $1{:}2_{[001]}$ versus $1{:}2_{[111]}$ supercells. The *unrelaxed* structure has an ideal axial ratio $\xi = 1$ and ideal perovskite atomic positions, but a lattice constant that minimizes the supercell total energy. On the other hand, the lattice constant, the axial ratio and the internal coordinates are all optimized in the *relaxed* calculations. One can clearly see that heterovalent and homovalent alloys differ. In both of the heterovalent compounds BZN and PZN, the unrelaxed $1{:}2_{[111]}$ supercell is lower in energy by more than 2.5 eV than the unrelaxed $1{:}2_{[001]}$ supercell. In homovalent PZT, on the other hand, neglecting the relaxations leads to a nearly identical total energy in the $1{:}2_{[001]}$ and $1{:}2_{[111]}$ supercells. This energetic difference between heterovalent and homovalent alloys can be understood in terms of a model recently developed to explain atomic ordering in perovskite alloys[30]. In this model, the total energy of a perovskite with B-site compositional freedom is approximated by an electrostatic energy given by

$$E = \frac{e^2}{2\epsilon a} \sum_{l \neq l'} \frac{\Delta q_l \Delta q'_l}{|\mathbf{l} - \mathbf{l}'|} \ , \tag{1}$$

where a is the cubic lattice constant and l runs over the *ideal* positions of the B atoms (e.g., over Zn and Nb atoms in BZN and PZN, or Zr and Ti atoms in PZT). ϵ is a electronic dielectric constant providing some screening effects and Δq_l is the relative charge, with respect to the average B charge, of the B atom in cell l. For example, since Zr and Ti belong to the same column (IV) of the periodic table, Δq_l is exactly zero for any cell in PZT. Applying Eq. [1] to PZT then leads to an energy that is independent of the atomic ordering between Zr and Ti atoms. As shown in Fig. 2c, this expectation is nearly exactly demonstrated in our calculations on the unrelaxed $1{:}2_{[001]}$ and $1{:}2_{[111]}$ structures. On the other hand, in both PZN and BZN, Δq is equal to $+1$ and -2 for Nb and Zn atoms respectively. Thus, the electrostatic energy E strongly depends on the atomic ordering of the B atoms, as demonstrated in Figs. 2a and 2b for the unrelaxed heterovalent supercells.

One can also evaluate the difference in energy between the *unrelaxed* $1{:}2_{[001]}$ supercell and the *unrelaxed* $1{:}2_{[111]}$ supercell for the heterovalent case (BZN or PZN) using the model of Eq. [1]. The result is that the unrelaxed $1{:}2_{[001]}$ structure is higher in energy than the unrelaxed $1{:}2_{[111]}$ structure by (5.274 a.u.)$/\epsilon a$. Fitting this formula to the first-principles energetic difference between the $1{:}2_{[111]}$ and the $1{:}2_{[001]}$ unrelaxed structures leads to reasonable values of the dielectric constant ϵ (6.3 in BZN and 7.5 in PZN). Thus, analyzing the first-principles results in the framework of this electrostatic model suggests that the screening is larger in Pb-heterovalent than in Ba-heterovalent compounds. This explains why the energy separation between unrelaxed $1{:}2_{[111]}$ and $1{:}2_{[001]}$ supercells is larger in BZN than in PZN.

We consider next the relaxation energies (including relaxation of both atomic and lattice degrees of freedom). Is is interesting to note that relaxations provide a comparable decrease in energy (0.6 eV-0.9 eV) in all three $1{:}2_{[111]}$ supercells, independently of both the B-atom valence and the A-atom kind. On the other hand, the relaxation energy in the $1{:}2_{[001]}$ supercell is strongly dependent on chemical effects. For instance, relaxing atomic and lattice degrees of freedom in the Pb-heterovalent alloy PZN leads to a gain in energy as large as 3.2 eV. This gain is 8 times larger than the corresponding relaxational decrease in the Pb-homovalent alloy PZT. As shown in Fig. 2, the different energetic behavior between Pb-homovalent and Pb-heterovalent $1{:}2_{[001]}$ cells has two direct consequences:

(i) The relaxed PZT $1{:}2_{[111]}$ is much more stable (by 0.4 eV) than the relaxed PZT $1{:}2_{[001]}$. A similar energetic decrease of 0.3 eV has also been calculated in Ref.[10] for a PZT alloy with 50% of Zr and 50% of Ti, when going from $1{:}1_{[001]}$ to $1{:}1_{[111]}$ B-site cation ordering. (Consistent with our previous notation, the $1{:}1_{[001]}$ structure exhibits a succession of two different B planes along the [001] direction.)

(ii) The relaxation occurring in PZN leads to a destabilization of the $1{:}2_{[111]}$ supercell with respect to the $1{:}2_{[001]}$ one. The gain in energy by atomic and cell optimization in the PZN $1{:}2_{[001]}$ structure thus overcomes both the electrostatic energy difference of 2.5 eV between unrelaxed $1{:}2_{[001]}$ and $1{:}2_{[111]}$ PZN structures, and the relaxation energy of 0.6 eV in the PZN $1{:}2_{[111]}$ structure[38]. This may be consistent with the fact that, unlike many chemically similar heterovalent alloys, the ground states of Pb-heterovalent alloys such as PMN and PMT do not experimentally adopt a 1:2 ordering along a [111] direction. The destabilization of the $1{:}2_{[111]}$ supercell has also been found in PZN[11]: relaxed calculations performed on five different order structures predicted that the $1{:}2_{[111]}$ supercell was only the third lowest in energy of those studied.

Relaxation in the $1{:}2_{[001]}$ heterovalent BZN supercell also lowers the energy by a considerable amount (2.6 eV.) However, in contrast with PZN, this large decrease is not able to overcome the very large electrostatic difference between the unrelaxed $1{:}2_{[001]}$ and unrelaxed $1{:}2_{[111]}$ BZN supercells. This could be explained by our above estimates indicating a smaller dielectric constant in BZN than in PZN. Our relaxed LDA calculations thus indicate that in BZN the $1{:}2_{[111]}$ supercell is significantly lower in energy than the $1{:}2_{[001]}$, which is consistent with the fact that the ground-state structure observed in BZN (and in many similar Ba-heterovalent alloys) is the $1{:}2_{[111]}$ one[4,14–18].

B. Structural and dielectric effects

1. A-atom effects in heterovalent alloys: BZN vs PZN

One may now wonder what are the structural signatures and the dielectric consequences of the different relaxations that we find in the three materials under study. These are summarized in Table I.

First, Table I shows that the heterovalent alloys exhibit similar trends in lattice parameters. For example, in both BZN and PZN, the axial ratio is larger for the $1{:}2_{[001]}$ structure than for the $1{:}2_{[111]}$ one. In particular, the axial ratio of the $1{:}2_{[001]}$ structure is significantly larger than the ideal value of unity (by 5% and 2% in BZN and PZN, respectively). This points to the importance of lattice relaxation in heterovalent alloys. As usual in LDA calculations, the calculated lattice constants agree within 1-2% with the experimental lattice constants of 4.096 Å for BZN[39,40] and 4.04 Å for PZN[41], the experimental values having been measured at room temperature in the cubic paraelectric phase.

Furthermore, we find that all the atomic bonds in the $1{:}2_{[111]}$ structure are very similar in the BZN and PZN cases: (i) the A–O bonds range between 2.80 and 2.86 Å independently of the A atom (i.e., Pb *vs.* Ba); (ii) the Zn–O bond is lengthened (around 2.05 Å); and (iii) the Nb–O bonds are equally divided into a group with intermediate lengths (1.91 Å) and a group of longer bonds with lengths close to that of the long Zn–O bond.

The atomic bonds in the $1{:}2_{[001]}$ structure are also qualitatively similar between PZN and BZN. For example, one may notice four different features characterizing relaxed heterovalent $1{:}2_{[001]}$ structures with respect to relaxed heterovalent $1{:}2_{[111]}$ structures: (i) four short A_1–O bonds, ∼2.5-2.7 Å, that are much shorter than those expected from the sum of ionic radii[42] (2.70 and 2.82 Å for Pb–O and Ba–O bonds, respectively); (ii) four short Zn–O bonds, ∼2.0 Å; (iii) two very long Zn–O bonds, ∼2.2-2.4 Å, that are much longer than the 1.95 Å expected from ionic radii considerations[42]; and (iv) one short Nb–O bond of 1.8 Å.

The differences in atomic bonds between BZN and PZN arise mainly in the $1{:}2_{[001]}$ structure. For example, some Zn–O bonds are much longer in BZN $1{:}2_{[001]}$ than in PZN $1{:}2_{[001]}$; in particular, the Zn–O bond in BZN $1{:}2_{[001]}$ is ∼0.4 Å longer than the value of 1.95 Å expected in a purely ionic perovskite compound[42]. Similarly, some Pb–O bonds in PZN $1{:}2_{[001]}$ are shorter by more than 0.1 Å than the shortest Ba–O bonds in BZN $1{:}2_{[001]}$. The formation of very short Pb–O covalent bonds in PZN, and the existence of (unstable) anomalous long Zn–O bonds in BZN, are probably the main quantitative reasons for the larger relaxation energy found in PZN $1{:}2_{[001]}$ compared to BZN $1{:}2_{[001]}$.

Table I also shows the Born effective charges Z^* for BZN and PZN supercells, calculated along the compositional direction (i.e., along either [001] or [111]). One finds similar trends as in simple perovskite compounds[43], namely values close to +3.0 and +4.0 for Ba and Pb atoms, respectively. On the other hand, we find that the effective charges of the Nb atoms are much smaller (by 1-2 units) in the heterovalent alloy than in the paraelectric states of simple compounds such as $KNbO_3$ and $NaNbO_3$[43]. Posternak *et al.* have shown[44] that the lengths of Nb–O bonds can have a drastic effect on the effective charges: they found that the Z^* of Nb decreases by more than 2.5 units when going from the cubic paraelectric phase to the tetragonal ferroelectric phase of $KNbO_3$. Thus, the fact that Nb atoms have a much smaller effective charge in BZN and PZN than in simple paraelectric compounds may be attributable to the Nb–O bond length distribution found in the alloys. Furthermore, as seen in Table I, the existence of very short Pb–O bonds, which have been experimentally detected in Pb-heterovalent alloys[31,45], also has a dielectric consequence: the effective charge of the Pb atom involved in those Pb–O bonds decreases when going from PZN $1{:}2_{[111]}$ to PZN $1{:}2_{[001]}$. A similar decrease of the Pb effective charge has already been seen when going from a system with "normal" Pb–O bonds to a system with short Pb–O bonds[9]. Similarly, heterovalent $1{:}2_{[001]}$ structures exhibit both longer Zn–O bonds and a decrease of the effective charge of the Zn atom.

2. Heterovalent effects: PZN vs PZT

As shown in Table I and at variance with heterovalent alloys, the homovalent PZT alloy adopts a near-ideal value of the axial ratio in both the $1{:}2_{[001]}$ and $1{:}2_{[111]}$ structures. The relaxation energy occurring in PZT $1{:}2_{[001]}$ is mainly attributable to the existence of longer Zr–O bonds and shorter Ti–O bonds, since the Pb–O bonds are very close to their unrelaxed value of 2.80 Å. Unlike the $1{:}2_{[001]}$ PZT and the $1{:}2_{[111]}$ BZN and PZN structures, the $1{:}2_{[111]}$ PZT structure exhibits short Pb-O bonds; again, these are presumably responsible for the stabilization of the relaxed $1{:}2_{[111]}$ PZT supercell over its $1{:}2_{[001]}$ counterpart. From a dielectric point of view, these short Pb–O bonds lead to an effective charge in PZT $1{:}2_{[111]}$ that is smaller than in PZT $1{:}2_{[001]}$. The main difference in the effective charges of heterovalent *vs.* homovalent alloys concerns the B' atom (i.e., Zn in PZN and BZN *vs.* Zr in PZT). One can see from Table I that Zr has an anomalously large effective charge ∼6.5) with respect to its purely ionic value of +4. A similar large effective charge of Zr has been found in simple compounds and results from the weak hybridization of nominally unoccupied Zr 4*d* orbitals with the oxygen 2*p* orbitals[43]. On the other hand, since the 3*d* shell in Zn is *below* the Fermi level, hybridization between the O 2*p* and Zn 3*d* orbitals does not contribute to the effective charge. (Incidentally, we find that this hybridization is strong, as reported also in Ref.[11].) Hybridization between the O 2*p* and Zn 4*d* states could in principle contribute to Z^*, but the Zn 4*d* states are much higher in energy and therefore unlikely to contribute strongly. This explains the small values of the Zn effective charges displayed in Table I.

IV. CONCLUSIONS

We have performed accurate first-principles supercell calculations to investigate energetic, structural and dielectric effects in heterovalent and homovalent perovskite alloys.

Our main findings are that the energetics of the homovalent PZT alloy is mainly driven by atomic relaxation and covalent effects. A PZT structure can thus be stabilized via the formation of short Pb–O bonds. The formation of these short Pb–O bonds, which have been experimentally seen[31], leads to a decrease of the effective charge of the Pb atoms.

On the other hand, we find that the energetics of the heterovalent BZN alloys is mainly driven by electrostatic interactions among the Zn and Nb atoms. As shown in Ref[30], these electrostatic interactions lead to the stabilization of the 1:2 long-range-ordered structure along the [111] direction. This 1:2 structure does not exhibit any short A–O bonds, which is consistent with the fact that very short Ba–O bonds have not been detected (to our knowledge) in heterovalent perovskite alloys.

The situation in PZN is in between those of BZN and PZN, in the sense that the optimization of the cell parameters and the formation of short Pb–O bonds in PZN could overcome the large electrostatic interaction among the Zn and Nb atoms. The destabilization of the 1:2 structure along the [111] crystallographic direction can thus happen in PZN. As in PZT, the formation of these short Pb–O bonds leads to a decrease of the effective charge of the Pb atoms in PZN.

Finally, one drastic difference in dielectric properties between heterovalent and homovalent alloys concerns the effective charge of the larger B-site atom B$'$. While Zr exhibits anomalous large effective charge, the Born effective charge of the Zn atom is very close to its nominal value.

V. ACKNOWLEDGMENTS

We wish to thank H. Krakauer, M. Wensell, N. Marzari and A. García for useful discussions. This work is supported by the ONR grant N00014-97-1-0048. Cray C90 computer time was provided at the NAVO MSRC DoD HPC center.

[1] K. Uchino, *Piezoelectric Actuators and Ultrasonic Motors*, Kluwer Academic Publishers, Boston, (1996).

[2] T. Tanaka, *Ferroelectrics* **40**, 167 (1982).

[3] L.M. Sheppard, *Cer. Bull.* **71**, 85 (1992).

[4] M.A. Akbas and P.K. Davies, *J. Am. Ceram.* **81**, 670 (1998).

[5] S.-E. Park and T.E. Shrout, *J. Appl. Phys.*, **82**, 1804 (1997)

[6] D. Vanderbilt, *Current Opinions in Solid State and Materials Science*, **2**, 701 (1997)

[7] G. Saghi-Szabo, R.E. Cohen and H. Krakauer, *Phys. Rev. Lett.* **80**, 4321 (1998).

[8] N. Marzari and D. Vanderbilt, in *First-Principles Calculations for Ferroelectrics: Fifth Williamsburg Workshop*, R.E. Cohen, ed. (AIP, Woodbury, New York, 1998), p. 146.

[9] L. Bellaiche, J. Padilla and David Vanderbilt, in *First-Principles Calculations for Ferroelectrics: Fifth Williamsburg Workshop*, R.E. Cohen, ed. (AIP, Woodbury, New York, 1998), p. 11.

[10] G. Saghi-Szabo and R.E. Cohen, *Ferroelectrics* **194**, 287 (1997).

[11] M. Wensell and H. Krakauer, in *First-Principles Calculations for Ferroelectrics: Fifth Williamsburg Workshop*, R.E. Cohen, ed. (AIP, Woodbury, New York, 1998), p. 165.

[12] B.P. Burton and R.E. Cohen, *Phys. Rev. B* **52**, 792 (1995).

[13] B.P. Burton, R.P. McCormack, B.H. Toby, and E.K. Goo, *Ferroelectrics* **194**, 187 (1997).

[14] U. Treiber and S. Kemmler-Sack, *J. Sol. State Chem* **43**, 51 (1982).

[15] A.J. Jacobson, B.M. Collins, and B.E.F. Fender *Acta Cryst. B* **32**, 1083 (1976).

[16] S.M. Allen and J.W. Cahn, *Acta Metall.* **20**, 27 (1972).

[17] R. Guo, A.S. Bhalla, and L.E. Cross *J. Appl. Phys.* **75**, 4704 (1994);

[18] I.T. Kim, S.J. Chung and K.S. Hong, *Ferroelectrics* **173**, 125 (1995).

[19] E. Husson, *Mat. Res. Bull.* **25**, 539 (1990).

[20] E. Husson, *Mat. Res. Bull.* **23**, 357 (1988).

[21] J. Chen, *J. Am. Cer. Soc.* **72**, 593 (1989).

[22] M.A. Akbas and P.K. Davies, *Journal of Materials Research.* **12**, 2617 (1997).

[23] W. Zhong, D. Vanderbilt and K.M. Rabe, *Phys. Rev. Lett.* **73**, 1861 (1994); *Phys. Rev. B* **52**, 6301 (1995).

[24] U. Waghmare and K. Rabe, *Phys. Rev. B* **55**, 6161 (1997).

[25] H. Krakauer, R. Yu, C.-Z. Wang and C. LaSota, *Ferroelectrics* in press (1997).

[26] J. Padilla, W. Zhong and D. Vanderbilt, *Phys. Rev. B* **53**, R5969 (1996).

[27] A. García and D. Vanderbilt, in *First-Principles Calculations for Ferroelectrics: Fifth Williamsburg Workshop*, R.E. Cohen, ed. (AIP, Woodbury, New York, 1998), p. 53.

[28] A. García and D. Vanderbilt, *Appl. Phys. Lett.* **72**, 2981 (1998).

[29] K.M. Rabe and E. Cockayne, in *First-Principles Calculations for Ferroelectrics: Fifth Williamsburg Workshop*, R.E. Cohen, ed. (AIP, Woodbury, New York, 1998), p. 61. Also available at http://xxx.lanl.gov/abs/cond-mat/9804056.

[30] L. Bellaiche and D. Vanderbilt, *Phys. Rev. Lett.*, in press (1998).

[31] T. Egami, S. Teslic, W. Domowski, P.K. Davies and I.-W. Chen, *submitted* (1997).

[32] D. Vanderbilt, *Phys. Rev. B* **41**, 7892 (1990).

[33] R.D. King-Smith and D. Vanderbilt, *Phys. Rev. B* **49**, 5828 (1994).

[34] D.M. Ceperley and B.J. Alder *Phys. Rev. Lett.* **45**, 566 (1980).

[35] J. Perdew and A. Zunger *Phys. Rev. B* **23**, 5048 (1981).

[36] H.J. Monkhorst and J.D. Pack, *Phys. Rev. B* **13**, 5188 (1976).

[37] R.D. King-Smith and D. Vanderbilt, *Phys. Rev. B* **47**, 1651 (1993).

[38] In contrast, M. Wensell and H. Krakauer (private communication) find a LDA relaxation energy for $1{:}2_{[001]}$ PZN which is about 10 % smaller than ours, leaving the $1{:}2_{[111]}$ structure slightly lower in energy. The reasons for this discrepancy are not currently fully understood.

[39] M. DiDomenico and S.H. Wemple, *J. Appl. Phys.* **40**, 720 (1969).

[40] S. Nomura and H. Arima, *Japan J. Appl. Phys.* **11**, 358 (1973).

[41] V.A. Bokov and I.E. Mylnikova, *Soviet Physics Solid State* **2**, 2428 (1961).

[42] CRC Handbook of Chemistry and Physics, CRC Press, Boca Raton New York, Ed. D. R. Lide (1998), and references therein.

[43] W. Zhong, R.D. King-Smith and D. Vanderbilt, *Phys. Rev. Lett.* **72**, 3618 (1994).

[44] M. Posternak, R. Resta and A. Baldereschi, *Phys. Rev. B*

50, 8911 (1994).
[45] I.-W. Chen, P. Li and Y. Wang, *J. Phys. Chem. Solids* **57**, 1525 (1996).

TABLE I. Lattice parameters a_0 and ξ (see text), atomic distances d, and effective charges Z^* of $Ba(Zn_{1/3}Nb_{2/3})O_3$ (BZN), $Pb(Zn_{1/3}Nb_{2/3})O_3$ (PZN), and $Pb(Zr_{1/3}Ti_{2/3})O_3$ (PZT) supercells. A_1 is an A atom that relaxes along the compositional direction, while A_2 is prevented from relaxing from its ideal position by symmetry. B' is the larger B atom (Zr in PZT, Zn in BZN and PZN); B'' is the smaller one (Ti in PZT, Nb in BZN and PZN.) For each kind of bond, the number of them occuring per supercell is indicated in brackets. Our calculations agree with the results of Ref.[11] within 0.04 Å for all the bond lengths of the PZN $1{:}2_{[111]}$ structure.

	BZN		PZN		PZT	
	$1{:}2_{[001]}$	$1{:}2_{[111]}$	$1{:}2_{[001]}$	$1{:}2_{[111]}$	$1{:}2_{[001]}$	$1{:}2_{[111]}$
a_0 (Å)	4.02	4.02	3.97	4.02	3.97	3.97
ξ	1.05	1.00	1.02	0.98	1.00	1.00
d(A_1–O) (Å)	2.66 [4]	2.85 [3]	2.54 [4]	2.80 [3]	2.74 [4]	2.60 [3]
	2.91 [4]	2.85 [3]	2.87 [4]	2.82 [3]	2.81 [4]	2.81 [6]
	3.28 [4]	2.86 [6]	3.28 [4]	2.85 [6]	2.91 [4]	3.07 [3]
d(A_2–O) (Å)	2.81 [8]	2.83 [6]	2.74 [8]	2.80 [6]	2.76 [8]	2.76 [6]
	2.84 [4]	2.84 [6]	2.81 [4]	2.85 [6]	2.81 [4]	2.81 [6]
d(B'–O) (Å)	2.01 [4]	2.07 [6]	1.98 [4]	2.04 [6]	1.98 [4]	2.06 [6]
	2.38 [2]		2.19 [2]		2.11 [2]	
d(B''–O) (Å)	1.82 [1]	1.91 [3]	1.84 [1]	1.91 [3]	1.89 [1]	1.98 [3]
	2.01 [4]	2.06 [3]	1.99 [4]	2.05 [3]	1.93 [1]	2.00 [3]
	2.10 [1]		2.06 [1]		1.98 [4]	
$Z^*(A_1)$	3.10	3.08	3.48	4.44	4.04	3.78
$Z^*(A_2)$	2.49	2.20	3.43	3.34	3.53	3.41
$Z^*(B')$	2.24	3.16	2.59	2.95	6.69	7.76
$Z^*(B'')$	6.88	6.54	7.82	6.45	6.65	5.81